# Remarks on bond of GFRP rebars and concrete

Giulia Fava, Valter Carvelli*, Marco Andrea Pisani

*Department of Architecture, Built Environment and Construction Engineering, Politecnico di Milano, Piazza Leonardo da Vinci 32, 20133 Milan, Italy*

The paper presents and extensive investigation on the bond behaviour between GFRP (glass fibre reinforced polymer) rebars and concrete. Pull-out tests were performed on helically wrapped and sand coated GFRP rebars with a wide range of diameters. Nonlinear finite element simulations of the tests allowed determining the effective distribution of the bond stress in the development length and the debonding propagation. An analytical model was developed to have an accurate prediction of the stress distribution at the interface and results were assessed with the numerical ones. Finally, the outcomes were compared with the design equations for the development length of FRP bars suggested in some design codes to assess their reliability.

*Keywords:*
A. Glass fibres
B. Debonding
C. Finite element analysis (FEA)
D. Mechanical testing Concrete

## 1. Introduction

In the design practice of reinforced concrete structural elements, debonding of rebars is not allowed as collapse mechanism. One consequence in considering collapse for debonding is that the materials are not completely exploited up to their best performance. As an alternative, a way to increase the load carrying capacity of the structural element without changing the shape of the cross section or the amount of the reinforcement (and therefore guarantee the invariance in stiffness of the structural element under service loads) is to reduce the rebars diameter and therefore increase the contact area in the anchorage length, so that debonding does not occur any more (or occurs at higher stress levels).

The Eurocode 2 simply states that “the ultimate bond strength shall be sufficient to prevent bond failure” (paragraph 8.4.2. in Ref. [1]).

These simple observations justify the effort spent by researchers and manufacturers to improve the bond strength of FRP and in particular GFRP (glass fibre reinforced polymer) rebars to concrete (see e.g. Refs. [2–10]), to have an effective alternative to steel rebars in reinforcing concrete structural elements.

Achieving good bond strength from pultruded GFRP rebars is not an easy task because of their nature: a high strength unidirectional reinforcement placed inside a low strength polymeric matrix (i.e. a markedly orthotropic overall material).

An efficient method to have good bond strength in pultruded GFRP rebars is to coat their surface with coarse quartz sand [6].

The bond strength of steel rebars (homogeneous isotropic material) is improved by means of ribs or slightly projecting patterns placed on its surface, while something similar can be achieved for GFRP rebars (heterogeneous anisotropic material) by wrapping a helical yarn around the bar before resin polymerization to obtain a corrugated surface. This upgrade inevitably decreases the tensile strength of the GFRP rebar because the helical yarn bends the outmost glass fibres and has an effect on their parallelism which globally reduces the effectiveness [11]. On the other hand, an external ribbed surface can be created on GRFP rebar cutting into the bar after curing.

The first part of this article presents the results of an experimental campaign for the measurement of bond of helically wrapped and sand coated GFRP rebars. Pull-out tests were performed on a wide range of diameters.

These tests were then simulated, in the second part, by means of a nonlinear finite element analysis to determine the effective distribution of the bond stress in the development length and how debonding propagates when the limit value of this stress is reached.

In the third part, the numerical predictions were compared to those of a developed analytical model to verify the reliability of the latter.

* Corresponding author. Tel.: +39 02 23994354.
*E-mail address:* valter.carvelli@polimi.it (V. Carvelli).


Published Journal Article available at: http://dx.doi.org/10.1016/j.compositesb.2016.03.012

Finally, the outcomes were compared with the design equations for the development length of FRP bars suggested by current design codes to verify the reliability of these design rules.

In this research work the decrease of bond strength depending on the environment will not be taken into account.

## 2. Materials, specimens and experimental features

The GFRP bars were made of unidirectional E-glass fibres and vynilester resin. The manufacturing involves a combination of pultrusion and wrapping processes. The external surface of the bars has a spiral aramidic yarn wound along the length (pitch close to the nominal diameter) and quartz sand (Fig. 1) to increase bond to concrete. The bars considered in the investigation had nominal diameter: 8, 10, 12, 16, 20 and 25 mm.

The mechanical properties of the bars were verified experimentally (see Ref. [11]). The average (three tests for each diameter) longitudinal tensile strengths of the bars are summarized in Fig. 2 for some diameters, while the elastic modulus for all diameters is 39 GPa.

Bond strength between concrete and the GFRP bars was experimentally measured by pull-out tests, according to the standard for steel rebars in concrete [12]. Concrete cubes of 200 mm side length were cast around GFRP bars. The geometry of the specimen is shown in Fig. 3, where $\Delta$ is the bar free length from the bond zone to the grip tabs, and $\varnothing$ is the bar nominal diameter. The length of bond surface between bar and concrete was selected according to the standard as $L = 5\varnothing$, wrapping PTFE foils (Poly-TetraFluoroEthylene) on the bar (see Fig. 3b).

Four concrete samples were preliminary tested to measure the concrete mechanical properties at room conditions. The compressive tests provided average cubic strength of 33.4 MPa with a standard deviation of 1.2 MPa.

The adopted pull-out test setup fulfils the suggestions of standard [12]. This arrangement produces a compressive transfer of the load to the concrete block with a steel plate (Fig. 4). As consequence, a confinement of the specimen is introduced which gives an influence on the failure mode (e.g. constrain to splitting). To allow dilatation of the concrete in the direction perpendicular to the bar, a PTFE sheet was positioned between the steel plate and the concrete specimen. This arrangement does not eliminate the confinement but reduces its influence. A mechanical testing machine with maximum load capacity of 500 kN was used (Fig. 4a). The cross-head displacement rate was set to 1 mm/min. A spherical hinge was used to correct small misalignments (Fig. 4b). Two displacement transducers (LVDT) were placed on the top cross section of the bar and of the concrete cube to measure the relative displacement between the steel frame and the unloaded end of the bar and between the steel frame and the concrete block (Fig. 4c). The difference of the two relative displacements provides the slip between bar and concrete.

## 3. Experimental results

Five specimens were tested for each bar diameter. Representative load vs. slip curves are depicted in Fig. 5 for the three highest diameters of GFRP bar. The solid lines in Fig. 5 refer to experimental data, while the dashed one represents the results of the numerical model presented in the following section. In the first part of the curves, the load has a linear increase up to the maximum load with almost null slip, while, in the second part, a non-linear response was observed with decreasing load and increasing slip up to complete debonding and sliding of the bars.

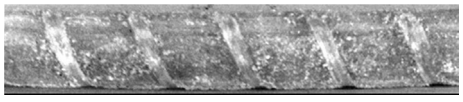

**Fig. 1.** External surface of GFRP bar, diameter 16 mm.

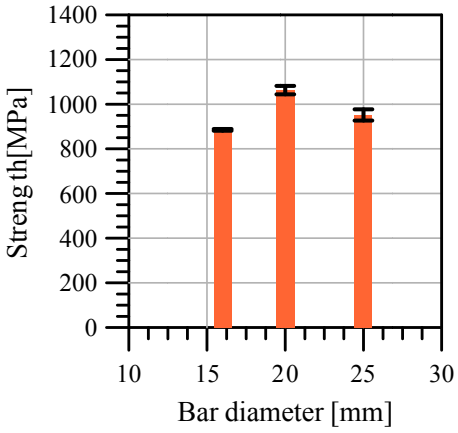


**Fig. 2.** Average tensile strength of the considered GFRP bars. Error bar means standard deviation of three tests.

The experimental results are collected in Fig. 6 in terms of the mean value (five tests for each diameter) of the maximum average shear stress ($\tau_{max}$). The average shear stress was calculated with reference to the bonded surface of the GFRP bar assuming the nominal perimeter of the bar cross section and the adhesion length of five diameters.

In Fig. 6 the average adhesive shear stresses for the GFRP rebars is moreover compared to those of some steel rebars. The steel rebars of grade B450C had nominal diameter of 8, 12 and 16 mm. Their average relative rib area $f_R$, according to [13], was 0.067, 0.083 and 0.082, respectively. The same geometry of the pull-out spec-imen, the same concrete quality and experimental setup were adopted for the steel rebars. GFRP bars ensure bond strength of the same level of the steel ones for the considered diameters.

The main difference of the GFRP and steel bond to concrete was the failure mode. The bond with GFRP failed at bars interface for all diameters (Fig. 7). The bars external layer, including the spiral aramidic yarn and quartz sand, was completely detached and the bar portion in contact with concrete shows a very smooth surface. On the other hand, the steel bars of lower diameters (8 and 12 mm) generated failure of the concrete at the interface, while split of the concrete cubes were observed using bars of diameter 16 mm (see Fig. 8).

These experimental results suggest a question that should be addressed, i.e. what is the optimal value of the development length of a GFRP rebar? The strength of a GFRP rebar approximately doubles with respect to steel rebars and the experimental data on pull-out specimens are similar to one another, therefore one could argue whether bond length should double too.

## 4. Numerical modelling

Finite element models were presented in the literature to predict and better understand the behaviour of the bond between the GFRP rebars and concrete (see e.g. Ref. [14]). In the present investigation, the software ABAQUS [15] was adopted for the numerical investigation considering three different diameters of the GFRP rebars.

The geometric solid models contain two parts: the GFRP bar and the concrete block. At first, both an axisymmetric model (Fig. 9a)

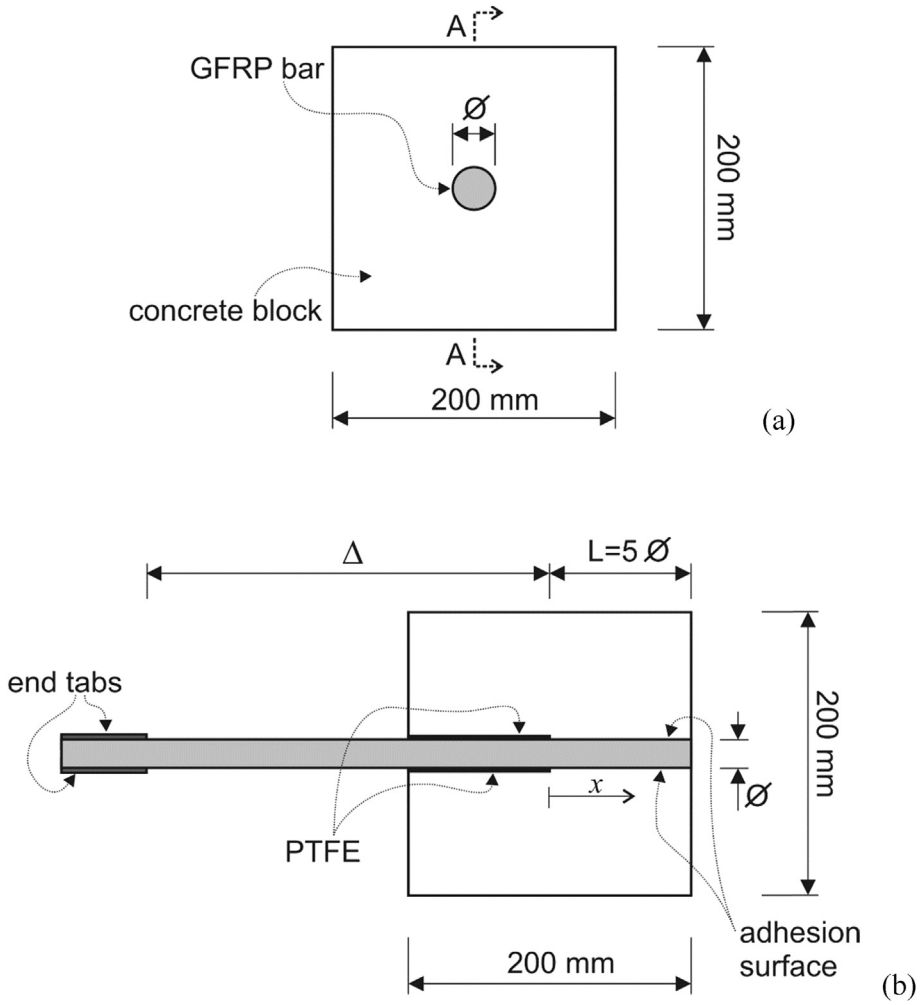


**Fig. 3.** Pull-out specimen geometry: (a) top view; (b) longitudinal section A–A.

and a more refined 3D model (Fig. 9b) were adopted for the analysis of the pull-out specimens with 16 mm diameter bars. The 3D model is limited to one quarter of the sample. The geometry of the pull-out specimen presents two planes of symmetry. The enforced boundary conditions reproduce the symmetries. In both models, the displacement of the bottom surface of the concrete block was constrained to reproduce the experimental setup. Axisymmetric four-node elements (CAX4R) and eight-node brick elements (C3D8R) were respectively used in the numerical models [15]. Details concerning the mesh assemblages are summarized in Table 1.

The constitutive laws of the materials are assumed to be linear elastic. The concrete was considered isotropic and elastic. The latter assumption is based on the fact that no cracks were observed during the experimental tests. The concrete had 30 GPa Young's modulus and Poisson ratio of 0.3. The elastic transversally isotropic GFRP bars were modelled considering theoretical mechanical properties [16] and assuming a fibre volume fraction of 50%. Their elastic modulus was 40 GPa in the longitudinal direction ($x$ in Fig. 9) and 8.6 GPa in the radial direction; the shear modulus was 3.39 GPa in the planes $x–z$ and $x–y$ and equal to 18 GPa in the plane $y–z$ (see Fig. 9), major and minor Poisson ratios were 0.28 and 0.1, respectively.

In the finite element analyses an increasing displacement up to 1.2 mm was applied at the loaded end section of the GFRP bar. The models allowed predicting the stress distribution at the interface, the corresponding load applied at the loaded end section of the GFRP bar and the slip, i.e., the relative displacement between the GFRP bar and concrete.

In the experimental investigation, the failure mechanism involved only the external layer of the rebars (see Fig. 7), while concrete at the interface was not damaged. Therefore, in both the 2D and 3D numerical simulations, the progressive debonding at the GFRP bar and concrete interface was simulated. The onset and growth of an interfacial crack were analysed by adopting fracture mechanics through an estimation of the critical energy release rates (ERR) for the mode I component due to opening tension ($G_I$), the mode II component due to in-plane shear ($G_{II}$) and the mode III component due to out-of-plane shear ($G_{III}$). Then, based on the Virtual Crack Closure Technique (VCCT) failure criterion, strain energy release rates at the crack tip were computed [17]. The VCCT, originally developed by Rybicki and Kanninen [18], is an appropriate crack propagation criterion for problems where brittle crack development occurs along predefined surfaces and is based on the assumption that the strain energy released when the crack is extended by a certain amount is the same as the energy required to close the crack by the same amount. The critical energy release rates for modes I, II and III were fixed after [19]. In detail, the ratios $G_{II}/G_I = 10$ and $G_{II}/G_{III} = 1$ were chosen, i.e., the ERR for mode I is considered to be negligible with respect to the ERR for mode II and

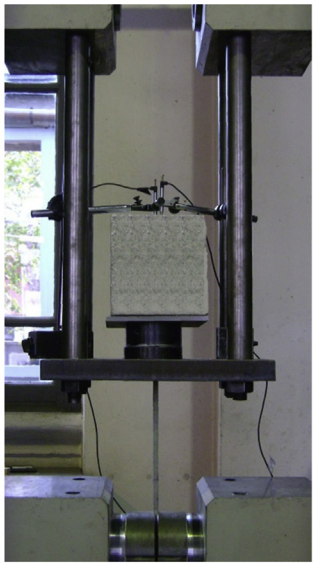

(a)

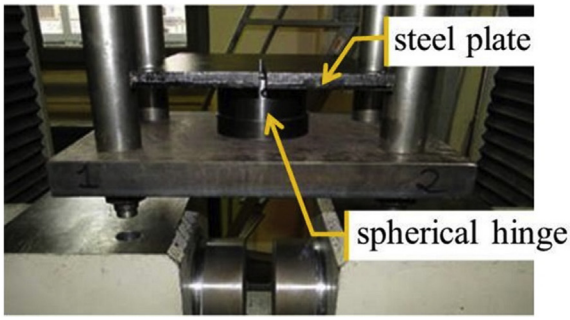


(b)

(c)

**Fig. 4.** Pull-out experimental set-up: (a) metallic frame for specimen position, (b) spherical hinge, (c) LVDTs for measurement of the slip.

the ERR is the same for modes II and III. The ERR values were then calibrated on the basis of the experimental curves (see Fig. 5). ERR values of 0.2 $N \cdot mm/mm^2$, 2 $N \cdot mm/mm^2$ and 2 $N \cdot mm/mm^2$ were thus found for modes I, II and III, respectively. Such values are comparable to the ones obtained in Ref. [20] for E-glass fibres embedded in a Portland cement.

For both the 2D and 3D models with 16 mm diameter bar, the numerical simulation allowed following the progressive debonding at the GFRP bar and concrete interface. In both cases, three values of the displacement applied at the loaded end section of the GFRP bar were taken into account: (a) for an applied displacement of 0.69 mm, no debonding was observed, (b) for an applied displacement of 0.77 mm, no debonding occurred and the maximum shear stress was reached and (c) for an applied displacement of 0.84 mm, a 12 mm long debonded zone was obtained. The results in terms of shear stresses at the concrete–bar interface were compared in Fig. 10 (the position $x$ on the interface is referred to the $x$ axis in Fig. 3). The results of the axisymmetric finite element model are slightly higher than the ones of the 3D simulation, but the difference is relatively small. These outcomes led the authors to adopt the 2D model for the further analyses. The choice is moreover justified observing that in the present context the numerical analysis is useful: (a) to verify the debonding onset and propagation at the GFRP bar and concrete interface, (b) to detect the shear stress distribution at the interface and its maximum value and (c) to eventually identify critical zones, but not to exactly calculate the stresses in the specimen.

Details concerning the mesh assemblages in the axisymmetric finite element simulation for nominal diameters of 16 mm, 20 mm and 25 mm are summarized in Table 2. In Fig. 11, the shear stresses obtained at the concrete–bar interface using the 2D model are detailed. In all the cases the shear stresses are observed to increase up to a maximum value of about 40 MPa before debonding starts.

While performing these analyses it was observed that the elastic properties of the rebars markedly influence the shear stress distribution. To verify this statement the shear stress distribution already computed for a 16 mm diameter GFRP rebar (Fig. 11a) was compared with the outcomes of the computation made with a similar rebar that nevertheless has the elastic properties (Young and Poisson moduli) of a steel rebar (see Fig. 12). Note that neither the contact behaviour at the concrete–GFRP bar interface, nor the failure criterion nor the interaction properties were changed (although obviously they are markedly different when dealing with steel or GFRP rebar). This is to focus only on the effect of the elastic properties of the rebars.

As expected, it can be stated that the elastic properties of steel imply an improvement of the shear stress distribution on the interface (stresses are high on a wider zone of the bar) and an increase of the maximum tensile pull out force.

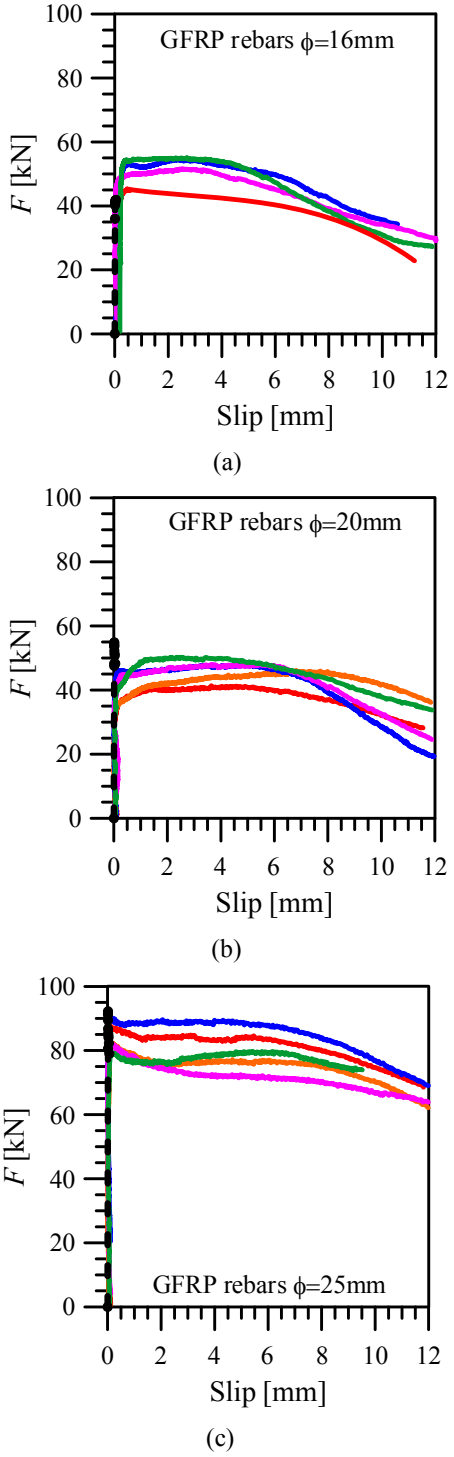


**Fig. 5.** Experimental and FEM load vs. slip curves of specimens with GFRP rebar of nominal diameter: (a) 16 mm; (b) 20 mm; (c) 25 mm. The solid lines refer to experimental data, the dashed one to the results of the numerical model.

This result can be interpreted assuming concrete as an elastic continuum bonded, along a segment of finite length, to an elastic restraint (the rebar). It is evident that the more the rebar is stiff, the more the shear stress tends to become constant along the development length (except than at its ends where abruptly drop to zero). This means that the resultant of the shear stress distribution of a GFRP rebar is lower than that of the same diameter steel rebar.

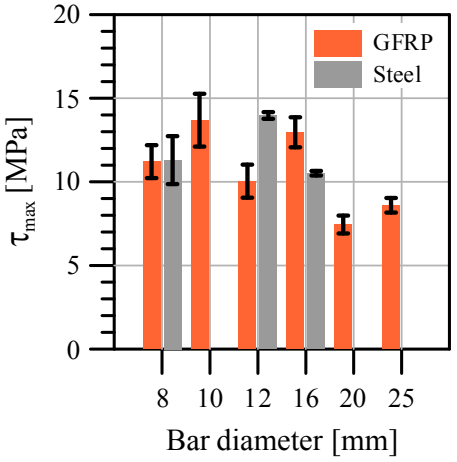


**Fig. 6.** Experimental maximum shear stresses ($\tau_{max}$) vs. GFRP bar nominal diameter. Comparison to steel rebars of nominal diameter 8, 12 and 16 mm. Average and standard deviation of five tests.

## 5. Analytical predictions

A reliable and fast prediction of the stress distribution along the contact development length is here obtained by an analytical model based on simplified assumptions.

In the literature more accurate models, than the one here presented, were proposed accounting for more complex relationships between the shear stress and the slip, see e.g. [20,21]. In Ref. [20], the bond-slip behaviour also accounts for a constant frictional shear stress along the debonding part of the composite reinforcement. In Ref. [21], a bond analytical formulation was presented by adopting a multilinear bond–slip relationship including elastic, plastic, softening and frictional phases.

In the GFRP/concrete system under analysis, a GFRP bar of diameter D is embedded in the concrete for a length equal to L (Fig. 3). Two different parts are distinguished: bond part (length $L-l$) and debonded part (length $l$). The debonding length $l$ is considered as the crack length at the interface.

The following assumptions are made, as in Refs. [20,22]:

- The concrete substrate is not deformable and is regarded as a rigid body, i.e., only the displacement of the GFRP bar in the concrete is taken into account.
- The materials are respectively homogeneous, isotropic and linearly elastic.
- In the bonded part, the shear stress $\tau$ at the GFRP/concrete interface is supposed, in a simple fashion, proportional to the GFRP displacement u, i.e. $\tau = ku$, where $k$ is the bond modulus. The bond–slip relationship reaches the maximum value $\tau_{max}$ at the onset of debonding (considered as crack tip) and then drops to zero (Fig. 13).

The equilibrium of a small length $dx$ of the GFRP bar (Fig. 3b) is:

$$\frac{dF(x)}{dx} = \tau(x)\pi D \quad \text{and} \quad F(x) = \int \tau(x)\pi D dx \tag{1}$$

Then, the strain in the GFRP rebar is:

$$\varepsilon(x) = \frac{\sigma(x)}{E} = \frac{4F(x)}{\pi D^2 E} = \frac{4\int \tau(x)dx}{DE} \tag{2}$$

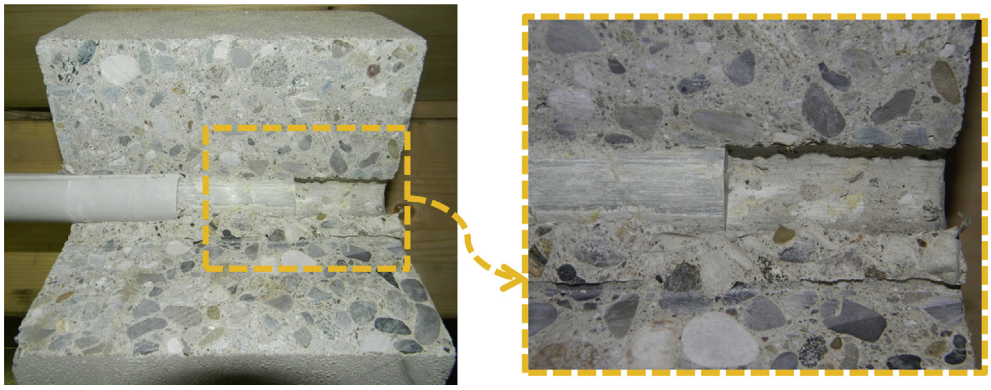

**Fig. 7.** Failure mode of a specimen with a GFRP bar of diameter 25 mm.


**Fig. 8.** Failure mode of a specimen with a steel bar of diameter 16 mm.

**Table 1**
Features of the finite element meshes (number of nodes and elements) for the axisymmetric model and the three dimensional model with 16 mm diameter GFRP bar.

| | | Bar diameter 16 mm | |
|---|---|---|---|
| | | Number of nodes | Number of elements |
| 3D model | GFRP | 1650 | 2576 |
| | Concrete | 28,300 | 33,366 |
| 2D model | GFR | 560 | 440 |
| | Concrete | 1285 | 1120 |

where $E$ and $\sigma$ are the Young's modulus and the tensile stress of the GFRP bar, respectively.

Considering the relationship between the longitudinal strain and the displacement in the GFRP rebar, i.e., $\varepsilon(x) = du(x)/dx$, the following equation is obtained:

$$\frac{d^2u(x)}{dx^2} - \frac{4\tau(x)}{DE} = 0 \tag{3}$$

Then, assuming the shear stress proportional to the GFRP displacement, one gets:

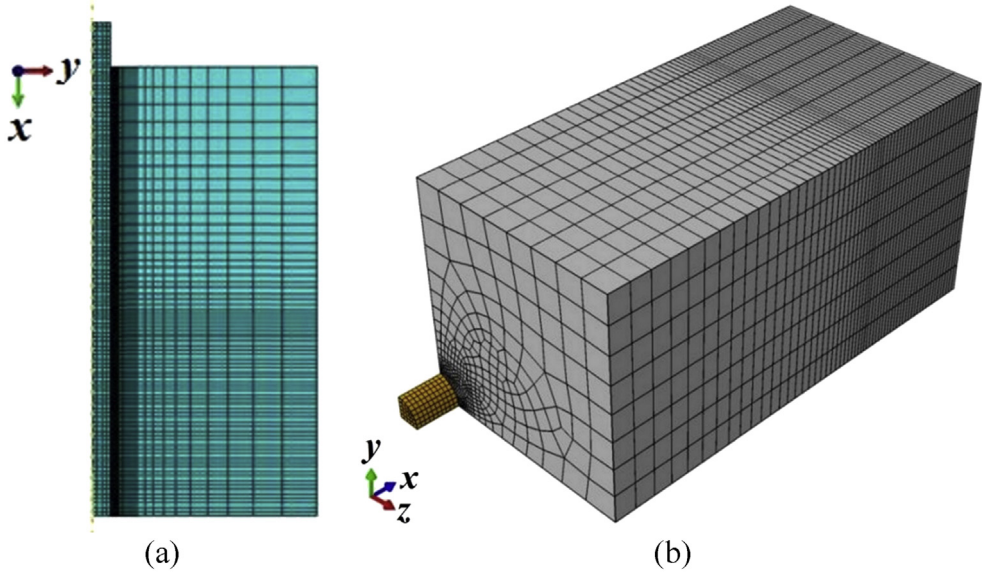


**Fig. 9.** (a) Axisymmetric and (b) 3D finite elements mesh adopted for numerical analyses.

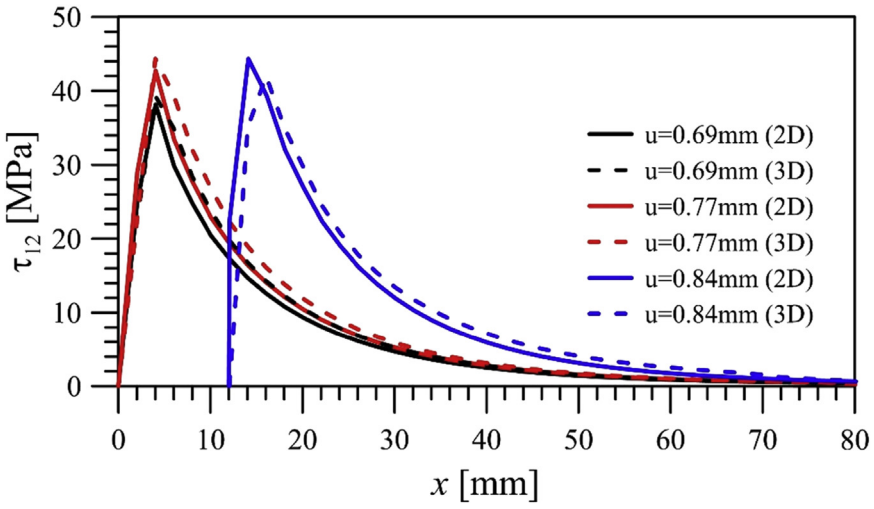


**Fig. 10.** Shear stresses at the concrete–bar interface for the 2D and 3D finite element simulations of pull-out test with a GFRP bar of diameter 16 mm.

**Table 2**
Features of the 2D finite element meshes (number of nodes and elements) for each diameter of GFRP bar considered.

| | | Bar diameter [mm] | | |
|---|---|---|---|---|
| | | 16 | 20 | 25 |
| GFRP bar | Nodes | 560 | 672 | 791 |
| | Elements | 440 | 550 | 666 |
| Concrete | Nodes | 1285 | 1349 | 1504 |
| | Elements | 1120 | 1170 | 1302 |

$$\frac{d^2u(x)}{dx^2} - \lambda^2 u(x) = 0 \quad \text{where } \lambda^2 = \frac{4k}{DE} \tag{4}$$

The integration of Eq. (4) gives:

$$u(x) = A\cosh(\lambda x) + B\sinh(\lambda x) \tag{5}$$

being $A$ and $B$ two constants.

Then the following boundary conditions are considered:

- At the free end of the bar the strain is null, i.e., $\varepsilon(x = L) = 0$;
- At the beginning of the embedded part ($x = 0$) the stress in the GFRP rebar is: $\sigma(x = 0) = 4F/\pi D^2$

The boundary conditions provide:

$$B = \frac{4F}{\pi D^2 E\lambda} \quad \text{and} \quad A = -\frac{4F}{\pi D^2 E\lambda}\frac{\cosh(\lambda L)}{\sinh(\lambda L)} \tag{6}$$

Finally, the following results are obtained:

$$\begin{aligned}
u(x) &= \frac{4F}{\pi D^2 E\lambda}\frac{1}{\sinh(\lambda L)}[\sinh(\lambda x)\cdot\sinh(\lambda L) - \cosh(\lambda x)\cdot\cosh(\lambda L)] \\
\varepsilon(x) &= \frac{4F}{\pi D^2 E}\frac{1}{\sinh(\lambda L)}[\cosh(\lambda x)\cdot\sinh(\lambda L) - \sinh(\lambda x)\cdot\cosh(\lambda L)] \\
\tau(x) &= \frac{4kF}{\pi D^2 E\lambda}\frac{1}{\sinh(\lambda L)}[\sinh(\lambda x)\cdot\sinh(\lambda L) - \cosh(\lambda x)\cdot\cosh(\lambda L)] \\
\sigma(x) &= \frac{4F}{\pi D^2}\frac{1}{\sinh(\lambda L)}[\cosh(\lambda x)\cdot\sinh(\lambda L) - \sinh(\lambda x)\cdot\cosh(\lambda L)]
\end{aligned} \tag{7}$$

For GFRP bars of diameter 16 mm, 20 mm and 25 mm, the bond modulus $k$ is found to be equal to 500 MPa/mm. Then, the shear stresses and the tensile stresses in the GFRP rebar were calculated for the following conditions: (a) bar diameter of 16 mm and applied load of 38 kN, (b) bar diameter of 20 mm and applied load of 48 kN and (c) bar diameter of 25 mm and applied load of 80 kN. The accuracy of the analytical model in predicting the stress distribution at the interface is highlighted by comparing the results to the numerical ones in Fig. 14.

## 6. Development length and current code provisions

Actually, in the authors' knowledge, among the existing rules and recommendations, the fib Bulletin 40 [23] is one of the most comprehensive codes for the definition of the basic development length of FRP reinforcing bars in concrete. Nonetheless, in the design of FRP RC sections, several critical points arise when dealing with the analysis of the bond between concrete and the FRP reinforcing bar.

As stated in Ref. [23], to ensure the proper development of the composite action in FRP RC structures and the successful transfer of forces from concrete to the reinforcement, a satisfactory bond length must be activated.

As observed in Section 4, the bond interaction of FRP bars is different from that of steel bars due to several reasons. In steel bars the interaction is mainly caused by the mechanical action of the bar lugs against concrete and, once the concrete tensile stress is exceeded, cracks start to develop and to propagate in the concrete substrate. FRP bars, instead, have a lower Young's modulus, a lower surface roughness and a lower strength of the peripheral surface under the coarse quartz sand (i.e. the resin), thus the bond interaction is primarily due to friction. As noticed in Section 3, when steel bars are used, bond failure occurs by concrete crushing, whereas peeling of the surface of the GFRP rebar was always observed.

Under this point of view, the approach proposed in Ref. [23] appears to be based on different assumptions, since bond failure between concrete and FRP reinforcing bars is considered to be largely caused by the partial failure in the concrete substrate or by splitting failure. Besides, some expressions for the bond evaluation in concrete elements have been proposed in Ref. [23], based on both the Japan Society for Civil Engineering (JSCE) recommendations on concrete structures with continuous fibre reinforcement [24] and

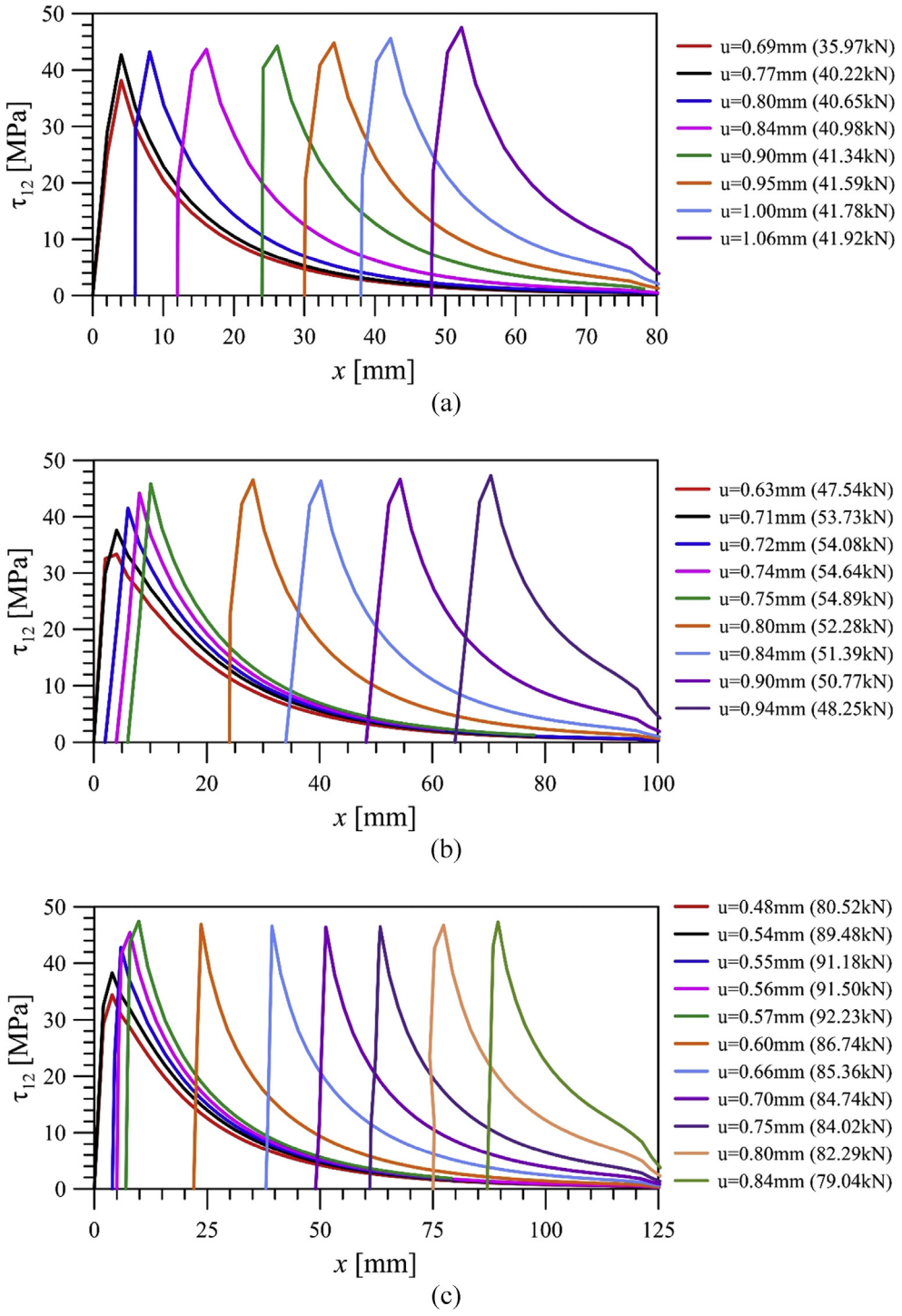


**Fig. 11.** Shear stresses at the concrete–bar interface for the 2D finite element simulations of specimens with a GFRP bar of diameter: (a) 16 mm, (b) 20 mm, (c) 25 mm.

the American Concrete Institute (ACI) design recommendations [25]. In both cases, the design of structural concrete using FRP bars is an extension of the code requirements for steel reinforced structures. In both formulations, the development length is calculated as a function of the ratio between the concrete cover or spacing $c$ and the bar diameter $d$: in Ref. [24] it is recognized that $c/d < 2.5$, while in Ref. [25] it is stated that if $c$ is larger than $d$, a pull-out failure may occur, otherwise splitting failure will be observed.

In detail, in Ref. [24] it is stated that, as a general rule, the basic development length of a FRP bar embedded in concrete should be experimentally obtained. In fact, as the development length depends on the reinforcement type, concrete strength, concrete cover and transverse reinforcement, tests should be performed to consider all such aspects. A formula for the bond splitting failure is finally proposed, but in any case the development length must be at least of 20 times the bar diameter. Pull-out tests are not considered to reflect bond characteristics in real members, since concrete provides a sufficient resistance to splitting because of the dimensions of the concrete cube and of the short embedment length of the rebar, thus the bond stress reaches the maximum average

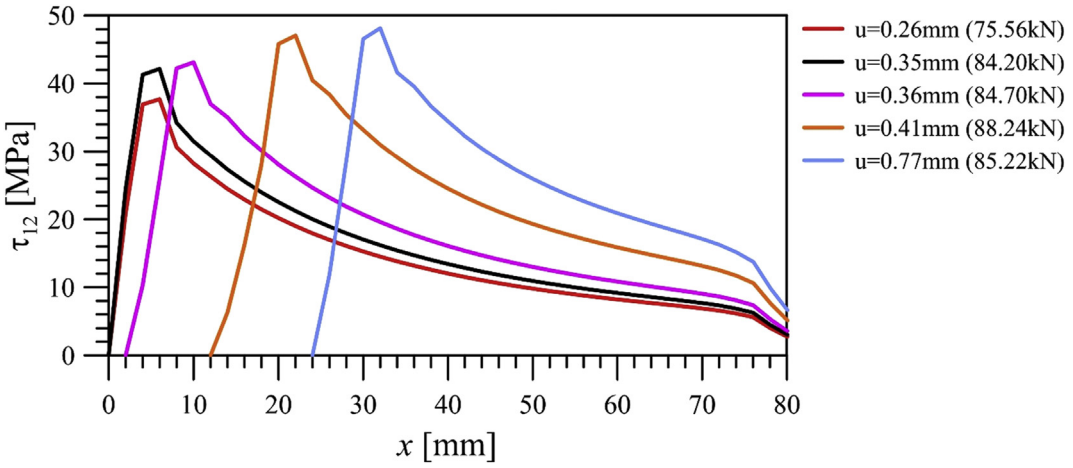


**Fig. 12.** Shear stresses at the concrete–bar interface for the 2D finite element simulations of specimen with a 16 mm diameter steel bar.

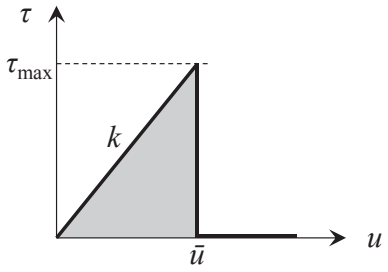


**Fig. 13.** Linear bond-slip law.

bond strength and the real bond strength is overestimated. Based on [24], the basic development length $l_0$ for FRP reinforcement is equal to:

$$l_0 = \frac{\left(\frac{f_y}{1.25\sqrt{f'_{cd}}} - 13.3\right) d}{0.318 + 0.795\left(\frac{c}{d} - \frac{15A_t}{sd}\right)} \tag{8}$$

where $f'_{cd}$ is the design compressive strength of concrete and $f_y$ corresponds to the design tensile strength of the FRP bar. The term $(15 \cdot A_t/(sd))$ represents the effect of the transverse reinforcement; where $A_t$ is the area of transverse reinforcement, $s$ is the distance between the centers of the transverse reinforcement and $d$ is the reinforcement bar diameter. Then, the bond stress of the FRP bar is evaluated considering Eq. (8) and the equilibrium of forces in the embedded length of the bar, so that:

$$f_{bod} = \frac{d}{4}\frac{f_y}{l_0} = \frac{0.318 + 0.795\left(\frac{c}{d} - \frac{15A_t}{sd}\frac{E_t}{E_0}\right)}{\left(\frac{3.2}{\sqrt{f'_{cd}}} - \frac{53.2}{f_y}\right)} \tag{9}$$

where $E_t$ is the Young's modulus of transverse reinforcement and $E_0$ is a standard Young's modulus for a steel bar (200 GPa). The JSCE recommendations additionally propose a comparison of the bond strength calculated following Eq. (9) with some experimental results, see Fig. 15. The experimental data of pull-out tests with GFRP bars that were discussed in this paper are added to the graph: a noticeable dispersion was found and for several experimental tests the bond strength appears to be almost three times greater than the corresponding estimated with Eq. (9).

Based on [25], the requirements for the design of concrete using FRP bars are analogous to the ones for steel reinforced structures. Besides it is explained that, if the concrete cover is larger than the bar diameter, a pull-out failure may occur, otherwise a splitting failure may occur. In any case, the proposed basic development length is calculated as:

$$l_d = \frac{\alpha \frac{\tau}{1.25\sqrt{f_c}} - 340}{13.6 + \frac{c}{d}} d \tag{10}$$

where $\tau$ is the bond stress to be developed, $f_c$ is the concrete compressive strength and $\alpha$ is a coefficient in the range between 1.0 and 1.4, depending on the reinforcement type.

Assuming the observations concerning the current codes, the experimental outcomes and the results from the numerical and analytical models, the following considerations arise:

- In the design formulae, the development length is not dependent on the Young's modulus of the FRP bar, while the FEM model shows that such parameter is extremely important for the definition of the area affected by the shear stresses at the interface between the bar and the concrete substrate, see Fig. 12.
- In all the design formulae, the development length is always influenced by the concrete compressive strength. On the other hand, as explained in Ref. [25] and as experimentally checked, under certain conditions concrete splitting is not observed while pull-out failure may occur.
- In Ref. [25], it is explained that the failure mode is influenced by the ratio between the concrete cover and the bar diameter but in the design expressions for calculating the development length the ratio $c/d$ is considered irrespective of the way the system is going to fail.
- In previous experimental researches ([26,27]) on strips of a real RC bridge slab, the authors stated that collapse in some cases occurred because of debonding of the rebars, but never occurred because of splitting or spalling, although the concrete cover was just 20 mm thick.

These remarks, together with the experimental and numerical analyses presented in the previous sections, allow to state that the

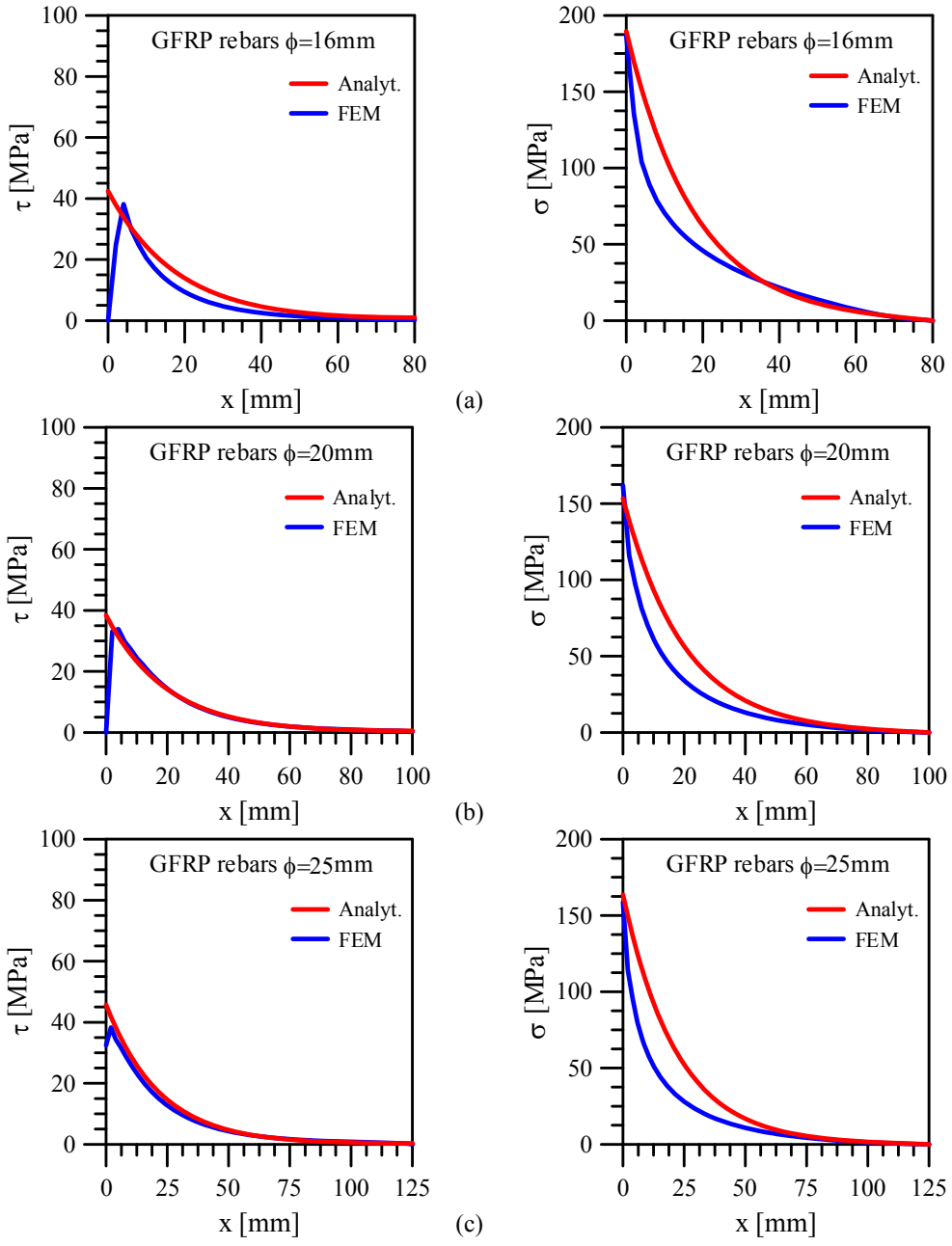


**Fig. 14.** Shear (τ) and normal stress (σ) at the concrete–bar interface based on the analytical model and on the 2D FEM simulation for GFRP bars of diameter: (a) 16 mm, (b) 20 mm, (c) 25 mm.

problem of the determination of the development length of FRP rebars is very complicated and not yet solved. The equations herein discussed have the merit of giving a method, although rough, to determine a development length, while other codes (such as for instance the Italian one) do not cover this topic.

## 7. Conclusions

The first target of this work was an in depth investigation on the behaviour of bond between concrete and GFRP rebars based on both laboratory tests and numerical modelling aimed to assess the evolution of the shear stress distribution over a progressing interface crack. The problem of the settlement of a reliable equation to determine the bond length of a GFRP rebar is still a question without a detailed answer, although based on the experimental and numerical evidences, reported in this paper, some remarks can be made.

- When dealing with steel rebars, debonding occurs because of concrete crushing around the ribs, or because of concrete splitting or spalling. The more bond strength increases and bond length shortens, the more the stress increases in concrete in the anchorage zone and therefore the more the concrete crushing, splitting and spalling problems are emphasized.
- The pull-out tests on GFRP rebars gave results comparable to those obtained for steel rebars although it can be stated that, when dealing with the considered system of GFRP rebars and concrete, failure occurs because of peeling of the bar instead of

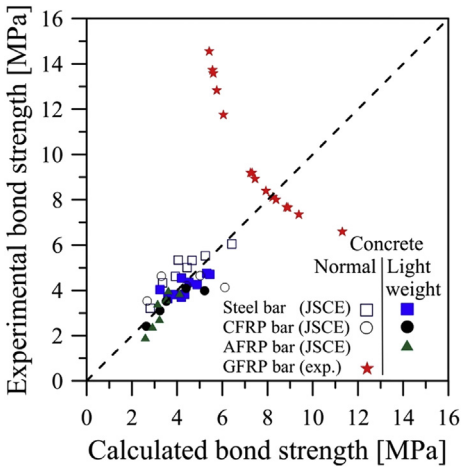


**Fig. 15.** Comparison of bond strength with test results on the basis of the JSCE recommendations; the stars refer to the experimental data discussed in this paper.

concrete crushing around it. This should imply both a decrease of the maximum bond stress (at debonding, concrete was not crushed or split jet), and a development length independent of the concrete strength.

- The FEM analyses show that the effective length, where an important bond stress acts, decreases together with the longitudinal elastic modulus of the rebar. This outcome should imply a further decrease of the effectiveness of bond of GFRP rebars with respect to steel ones.
- The Japanese and the American codes suggest determining a development length by means of the same equations already adopted for steel rebars (the only exception being minor changes), but do not satisfactorily interpret the experimental evidence.

All these statements suggest the need to revise the equations already available in order to propose more realistic formulas and effective in determining the development length of the GFRP rebars. The numerical and the analytical models presented here and others in the literature can give a very useful contribution in assessing the actual and future proposal for the development length of the GFRP rebars. This increases the confidence in adopting such GFRP reinforcement in concrete structural elements.

## Acknowledgement

The support of Sireg S.p.A. for the production of the GFRP rebars are gratefully acknowledged.

## References

[1] European Committee for Standardization (CEN). Eurocode 2: design of concrete structures – part 1–1: general rules and rules for buildings. EN 1992-1-1. 2005.
[2] Vilanova I, Baena M, Torres L, Barris C. Experimental study of bond-slip of GFRP bars in concrete under sustained loads. Compos Part B Eng 2015;74:45–52. http://dx.doi.org/10.1016/j.compositesb.2015.01.006.
[3] Lee JY, Yi CK, Cheong YG, Kim BI. Bond stress-slip behaviour of two common GFRP rebar types with pullout failure. Mag Concr Res 2012;64(7):575–91. http://dx.doi.org/10.1680/macr.11.00050.
[4] Choi DU, Chun SC, Ha SS. Bond strength of glass fibre-reinforced polymer bars in unconfined concrete. Eng Struct 2012;34:303–13. http://dx.doi.org/10.1016/j.engstruct.2011.08.033.
[5] Newman N, Ayoub A, Belarbi A. Development length of straight FRP composite bars embedded in concrete. J Reinf Plast Compos 2010;29(4):571–89. http://dx.doi.org/10.1177/0731684408100262.
[6] Baena M, Torres L, Turon A, Barris C. Experimental study of bond behaviour between concrete and FRP bars using a pull-out test. Compos Part B Eng 2009;40(8):784–97. http://dx.doi.org/10.1016/j.compositesb.2009.07.003.
[7] Hao Q, Wang Y, He Z, Ou J. Bond strength of glass fiber reinforced polymer ribbed rebars in normal strength concrete. Constr Build Mater 2009;23:865–71. http://dx.doi.org/10.1016/j.conbuildmat.2008.04.011.
[8] Okelo R, Yuan RL. Bond strength of fiber reinforced polymer rebars in normal strength concrete. J Compos Constr 2005;9(3):203–13. http://dx.doi.org/10.1061/(ASCE)1090-0268(2005)9:3(203).
[9] Balázs GL. Connecting reinforcement to concrete by bond. Beton Stahlbetonbau 2007;102:46–50. http://dx.doi.org/10.1002/best.200710109.
[10] Benmokrane B, Tighiouart B, Chaallal O. Bond strength and load distribution of composite GFRP reinforcing bars in concrete. ACI Mater J 1996;93(3):254–9. http://dx.doi.org/10.14359/9810.
[11] Carvelli V, Fava G, Pisani MA. Anchor system for tension testing of large diameter GFRP bars. ASCE J Compos Constr 2009;13(5):344–9. http://dx.doi.org/10.1061/_ASCE_CC.1943-5614.0000027.
[12] European Committee for Standardization (CEN). Steel for the reinforcement of concrete – weldable reinforcing steel – general. EN 10080. 2005.
[13] European Committee for Standardization (CEN). Steel for the reinforcement and prestressing of concrete – test methods – part 1: reinforcing bars, wire rod and wire. EN ISO 15630–1. 2010.
[14] Pepe M, Mazaheripour H, Barros J, Sena-Cruz J, Martinelli E. Numerical calibration of bond law for GFRP bars embedded in steel fibre-reinforced self-compacting concrete. Compos Part B 2013;50:403–12.
[15] ABAQUS standard user's manual, rel. 6.13. Dassault Systèmes Simulia; 2013.
[16] Daniel IM, Ishai O. Engineering mechanics of composite materials. New York: Oxford University Press; 1994.
[17] Kruger R. The virtual crack closure technique: history, approach and applications. NASA/CR-2000- ICASE Report No. NASA/CR-2002–211628. 2002.
[18] Rybicki EF, Kanninen MF. A finite element calculation of stress intensity factors by a modified crack closure integral. Eng Fract Mech 1977;9(4):931–8. http://dx.doi.org/10.1016/0013-7944(77)90013-3.
[19] Kruger R. Development and application of benchmark examples for mixed mode I/II quasi-static delamination propagation predictions. NASA/CR-2012–217562. NIA Report No. 2012-01.
[20] Zhang XB, Aljewifi H, Li J. Failure behaviour investigation of continuous yarn reinforced cementitious composites. Constr Build Mater 2013;47:456–64. http://dx.doi.org/10.1016/j.conbuildmat.2013.05.022.
[21] Mazaheripour H, Barros JAO, Sena-Cruz J, Soltanzadeh F. Analytical bond model for GFRP bars to steel fiber reinforced self-compacting concrete. ASCE J Compos Constr 2013;17(6). http://dx.doi.org/10.1061/(ASCE)CC.1943-5614.0000399.
[22] Yuan H, Teng JG, Seracino R, Wu ZS, Yao J. Full-range behaviour of FRP-to concrete bonded joints. Eng Struct 2004;26:553–65. http://dx.doi.org/10.1016/j.engstruct.2003.11.006.
[23] Fib bulletin 40, FRP reinforcement in RC structures. Lausanne: Fib – International Federation of Concrete; 2007.
[24] JSCE. Recommendation for design and construction of concrete structures using continuous fibre reinforcing materials. Tokyo, Japan: Research Committee on Continuous Fiber Reinforcing Materials, Japan Society of Civil Engineers; 1997.
[25] ACI Committee 440 ACI 440.1R-06-Guide for the design and construction of concrete reinforced with FRP bars. American Concrete Institute (ACI); 2006.
[26] Carvelli V, Pisani MA, Poggi C. Fatigue behaviour of concrete bridge deck slabs reinforced with GFRP bars. Compos Part B Eng 2010;41(7):560–7. http://dx.doi.org/10.1016/j.compositesb.2010.06.006.
[27] Carvelli V, Pisani MA, Poggi C. High temperature effects on concrete members reinforced with GFRP rebars. Compos Part B Eng 2013;54(1):125–32. http://dx.doi.org/10.1016/j.compositesb.2013.05.013.